# InAs Nanostructures for Solar Cell: Improved Efficiency by Submonolayer Quantum Dot

Najla Alanmi<sup>1</sup>, Rahul Kumar<sup>2</sup>\*, Andrian Kuchuk<sup>2</sup>, Yurii Maidaniuk<sup>1</sup>, Samir K. Saha<sup>3</sup>, Morgan E. Ware<sup>4</sup>, Yuriy I. Mazur<sup>2</sup>, Gregory J. Salamo<sup>2,3</sup>

Materials Science & Engineering, University of Arkansas, Fayetteville, AR 72701, USA
 Institute for Nanoscience and Engineering, University of Arkansas, Fayetteville, AR 72701, USA
 Department of Physics, University of Arkansas, Fayetteville, AR 72701, USA
 Department of Electrical Engineering, University of Arkansas, Fayetteville, AR 72701, USA

#### Abstract:

The effect of different quantum structures in the intrinsic region of a pin junction solar cell (SC) on the optical and electrical properties have been investigated. SCs with different quantum structures, such as, Stranski-Krastanov (SK) quantum dots (QDs), quantum well (QW), submonolayer (SML) QDs (0.25 ML, 0.5 ML and 0.75 ML) and a quasi-monolayer (1 ML) InAs stack, were fabricated while keeping the total InAs content the same in all SCs. In a comparison of performance, the SML-QD sample delivered superior performance (Almost 23% relative efficiency improvement compared to reference SC) compared to the other devices. These findings present a promising alternative to SK-QDs as intermediate band in photovoltaic applications.

#### 1. Introduction

The intermediate band solar cell (IBSC) concept was proposed to enhance the solar cell (SC) efficiency over the Schockley-Queisser thermodynamic limit of a single junction solar cell [1]. For example, the enhancement in efficiency can be accomplished by extending the solar absorption spectra of a semiconductor by capturing sub-bandgap photons via a narrow band of electronic states that exist within the semiconductor energy band gap. Efficiency enhancement by IBSC has been the topic of intense investigation and debate since its inception [2]–[8]. However, when adding an intermediate band to a SC, there is agreement that a quasi-fermi level discontinuity ( $\Delta$ QFL) is needed between the intermediate band and the conduction band, to maintain the open circuit voltage ( $V_{OC}$ ) of the SC [9].

One experimental realization of an IBSC utilizes vertical stacks of InAs Stranski-Krastanov (SK) QDs embedded in the intrinsic region of a GaAs pin diode [10] for the sub-bandgap electronic states. As a result, sub-bandgap photons absorbed in these solar cells promote carriers into the confined states. These carriers can then be extracted into the barrier's bands by either a second photon absorption, thermal escape or tunneling. By extending the solar absorption spectra, the short-circuit current (I<sub>SC</sub>) is therefore enhanced. Devices utilizing this strategy, unfortunately have suffered from degradation in open circuit voltage V<sub>OC</sub>, which has ultimately resulted in efficiency degradation in the SK QD [11] based IBSC [12]–[14]. Consequently, very few reports have shown even a slight enhancement in efficiency over the reference pin solar cell [14][15]. However, if the V<sub>OC</sub> degradation could be minimized, then the QD IBSC efficiency can be increased.

The main reasons for deteriorated efficiency of InAs SK QD based IBSC, are recapturing or trapping of excess carriers and strain-induced defects [16]. Trapping mainly depends on the QD size, where smaller QDs will result in reduced trapping [17]. However, this is a trade-off since smaller QDs decreases absorption bandwidth. To explore this trade-off we investigated submonolayer (SML) based InAs QD as an alternative method to the more conventional SK QD. Submonolayer QDs, achieve a much smaller QD size [18]–[20] and higher uniformity in size. SML-QDs are grown by depositing alternate layers of SML InAs (preferably 0.25-0.5ML) and thin Ga(In)As barriers. Several advantages of SML-QDs over SK-QDs are smaller size, higher dot density and uniformity [21].

This paper reports on an investigation of the comparative performance of different In(Ga)As quantum structure solar cells: (1)SK-QD, (2) SML QD (3) quantum well (QW) and (4) a quasi-ML InAs stack solar cell. Superiority of SML-QD based solar cell over both the SK-QD and the InGaAs QW based solar cell (SC), is found. Significant improvement in efficiency over the reference GaAs pin diode based solar cell is also observed. The effect of the different quantum structures (in the intrinsic region of the SC) on the structural, optical and electrical properties were studied by X-ray diffraction (XRD), photoluminescence (PL), external quantum efficiency (EQE), and illuminated current-voltage (I-V), respectively.

## 2. Experimental Measurements:

All samples were grown by conventional Molecular Beam Epitaxy (MBE) on n<sup>+</sup>-GaAs (001) substrates. In total, seven solar cell samples were fabricated. The reference GaAs solar cell (sample S1) without any quantum structure had a p-i-n structure with a 10 nm p<sup>+</sup>-GaAs contact layer, 30 nm p<sup>+</sup>-Al<sub>0.8</sub>Ga<sub>0.2</sub>As window layer, 400 nm p<sup>+</sup>-GaAs emitter layer, 330 nm undoped GaAs, 1 μm n-GaAs base layer, 100 nm n<sup>+</sup>-Al<sub>0.8</sub>Ga<sub>0.2</sub>As back surface field layer and 250 nm n<sup>+</sup>-GaAs buffer. For the SML-QDSCs, four different SML-QD stacks of InAs (0.25ML)/GaAs (1.25ML) (sample S2), InAs (0.5ML)/GaAs (2.5ML) (sample S3), InAs (0.75ML)/GaAs (3.75ML) (sample S4) and InAs (1ML)/GaAs (5ML) (sample S5) were grown in the undoped GaAs region. For the SK-QDSC (sample S6), 2ML InAs was separated by 20 nm GaAs. Finally, a SC sample with a stack of InGaAs QW (sample S7) was grown.

The total InAs content of ~30 ML was maintained for all samples containing InAs. The total thickness of undoped region was kept constant (330 nm) in all samples. Thickness and composition of epitaxial materials were controlled by reflection high energy electron diffraction (RHEED). For SK-QD sample, 2D-3D transition was also monitored by RHEED.

For PL measurements, the samples were mounted in a closed-cycle cryostat (Janis CCS-150) with variable temperature capability from 10 to 300 K. For the PL measurements, all samples were excited by a 532-nm continuous-wave (CW) laser. The PL signal was detected by a liquid nitrogen cooled CCD detector array (Princeton Instruments PyLoN: 1024-1.7) attached to a 50-cm focallength spectrometer (Action 2500).

XRD scans were performed on PANalytical X'Pert MRD diffractometer equipped with a multilayer focusing mirror, a standard four-bounce Ge (220) monochromator providing a collimated and monochromatic incident Cu K $\alpha$ 1 source of radiation ( $\lambda$ = 0.15406 nm), and a Pixel detector. In this case,  $\omega$ -2 $\theta$  scans, measured in the vicinity of GaAs (004) reflection, were used for characterization of the layer's thickness and strain. For device characterizations, AuGe/Ni/Au and Ti/AuZn/Au were used for back and front ohmic contacts, respectively, in 5 mm x 5 mm solar cells. No antireflection coating was applied to the samples.

The external quantum efficiency (EQE) measurement was performed at RT by QEX10 system with a xenon arc lamp source dispersed by a monochromator. The current-voltage (I-V) measurements were performed at RT under AM1.5 illumination with irradiance of 100 mW/cm<sup>2</sup>.

### 3. Result and Discussion:

# A. X-ray diffraction (XRD):

Fig. 1 (a) shows the symmetric (004)  $\omega$ -20 scans for all samples. Compared to the reference sample (S1), the periodic superlattice (SL) peaks can be clearly observed for all the samples, originating from periodic repetition of different quantum structures. These sharp interference fringes and well defined separation between them, give the information about the interface and the crystal quality. To further investigate the quality, rocking curves (RCs) of zeroth-order SL (SL0) peaks (marked with red arrow in Fig. 1(a)) are measured and shown in Fig. 1 (b). The linewidth of SL0 RCs and GaAs RCs are listed in the Fig. 1. Linewidth of SL0 peaks closely match with the GaAs RC linewidth for all samples indicating that the effect of defects dominates over the effect of interface roughness, in the RC linewidth. The SK-QD sample shows the smallest linewidth among all other samples. Strain relaxation due to surface modification could be the reason for a lower defect density and hence smallest linewidth in S6 compared to the other InAs samples. The 1ML InAs stack (S5) shows the highest linewidth. Bigger InAs Islands for the 1ML sample would result in higher strain and hence higher defects. Meanwhile, the slightly higher linewidth for S2 (0.25ML) sample, among other SML samples, may be because of higher strain due to vertical alignment of InAs islands which result in the formation of SML QD. We will discussion the differences in the RC when comparing SC performance.

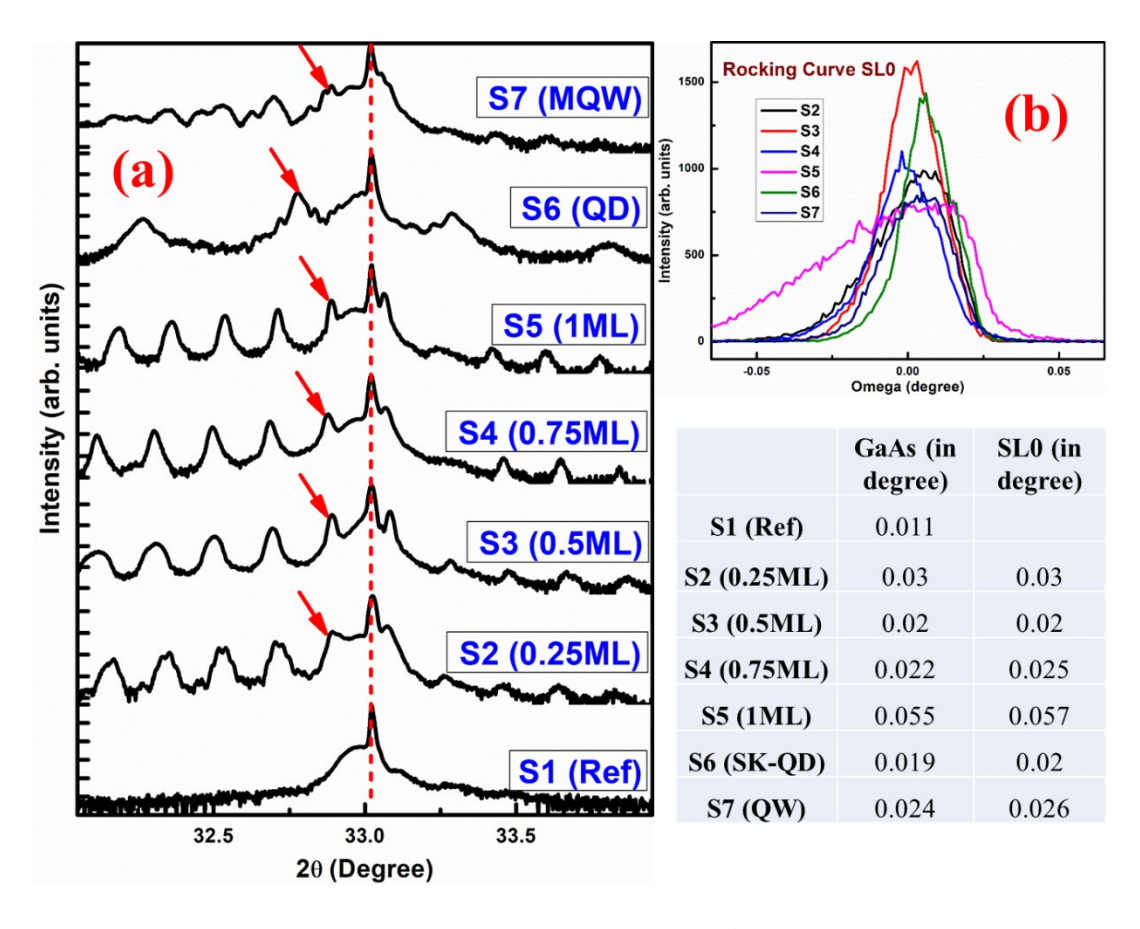


Fig. 1. (a) ω-2θ scans of all samples, red arrows show the 0<sup>th</sup> order SL peak (SL0) whereas red broken line shows the GaAs peak; (b) RCs for SL0 peak for all samples except S1; table shows the RC linewidth of GaAs and SL0 peaks.

## B. Photoluminescence (PL)

Fig. 2 shows the PL spectra of all InAs samples at low temperature (LT, 10 K) and at room temperature (RT, 300 K). Both at LT and RT, PL emission energy of S2 (0.25ML) and S3 (0.5ML) samples are higher than S4, S5 and S7. This is expected due to stronger carrier confinement. The PL peak position for SK-QD (shown in the inset) is further red-shifted compared to the other samples because of the larger size of the InAs QD formation compared to SML QDs. For the samples, the LT PL spectra shows a clear low energy tail while the RT PL spectra show a clear higher energy tail. The low energy tail in the LT PL spectra is due to the localized states often observed even for single SML InAs [22]. Meanwhile, the high energy tails in the RT PL spectra are mainly due to thermal broadening due to strong exciton-phonon interaction [11].

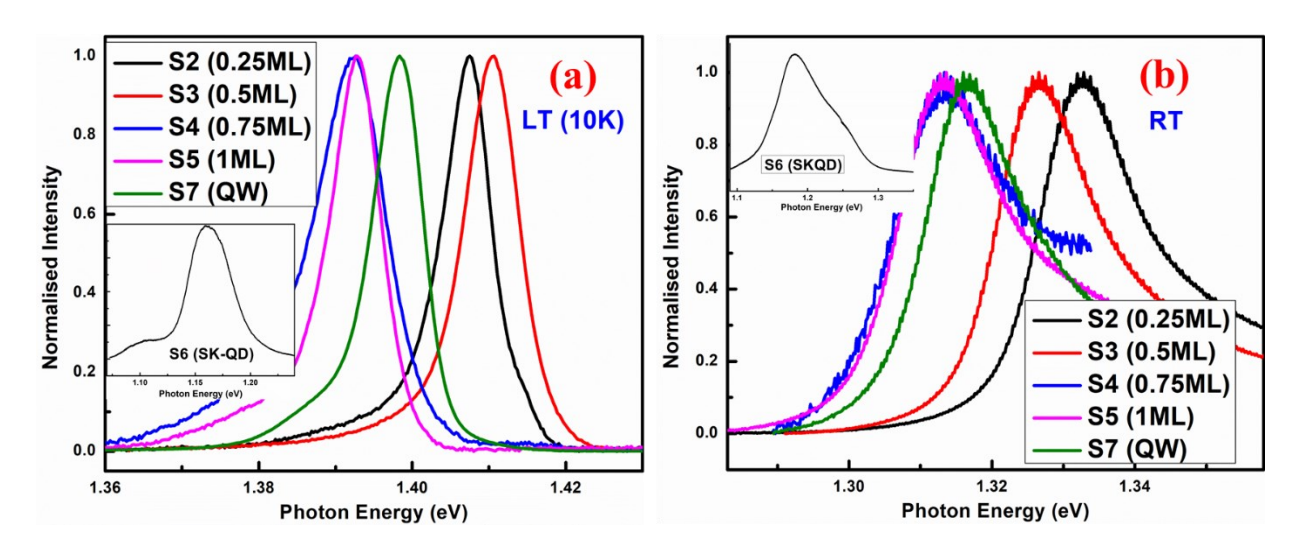


Fig. 2. (a) LT and (b) PL spectra of samples; inset of each plot shows the PL spectra of S6 (SKQD).

# C. External Quantum Efficiency (EQE)

Fig. 3 (a) shows the EQE spectra of all samples. The EQE spectra clearly shows the below bandgap (~1.4 eV) photon absorption by samples containing In(Ga)As, indicating the additional photocurrent generation compared to reference cell. As seen in Fig.3, the EQE behavior, as a function of photon energy, is different for different SCs. For the purpose of discussion, the SC spectra has been divided into three regions: I) region 1 (R1): EQE spectra for Sub-bandgap photons (shown in Fig. 3(b)), II) region 2 (R2): EQE spectra for above bandgap photons (shown in Fig. 3(c)), III) region 3 (R3): EQE spectra for high energy photons (shown in Fig. 3(d)).

For region 1, sample S2 (0.25ML) shows the highest EQE for sub-bandgap photons. More specifically, we observe higher absorption of sub-bandgap photons, and subsequent efficient carrier extraction, for S2. The EQE spectra peak is slightly blue shifted for S2 compared to other samples which is consistent with the RT PL.

For region 2, the SK-QD sample shows the lowest EQE in this region because of the carrier trapping by relatively large QDs. Again S2 shows the best behavior which is as good as the reference solar cell (S1) because of the reduced carrier trapping due to small size of SML QD.

For very high energy photons, or region 3, the EQE spectra (shown in Fig. 3 (d)) agree with the RC results. Since the 1ML sample (S5) shows the highest RC linewidth, EQE is lower for S5. S3

(0.5ML) while S6 (SK-QD) shows the higher EQE consistent with smaller RC linewidth. Hence, EQE behavior for high energy photons is dictated by defects in the GaAs material.

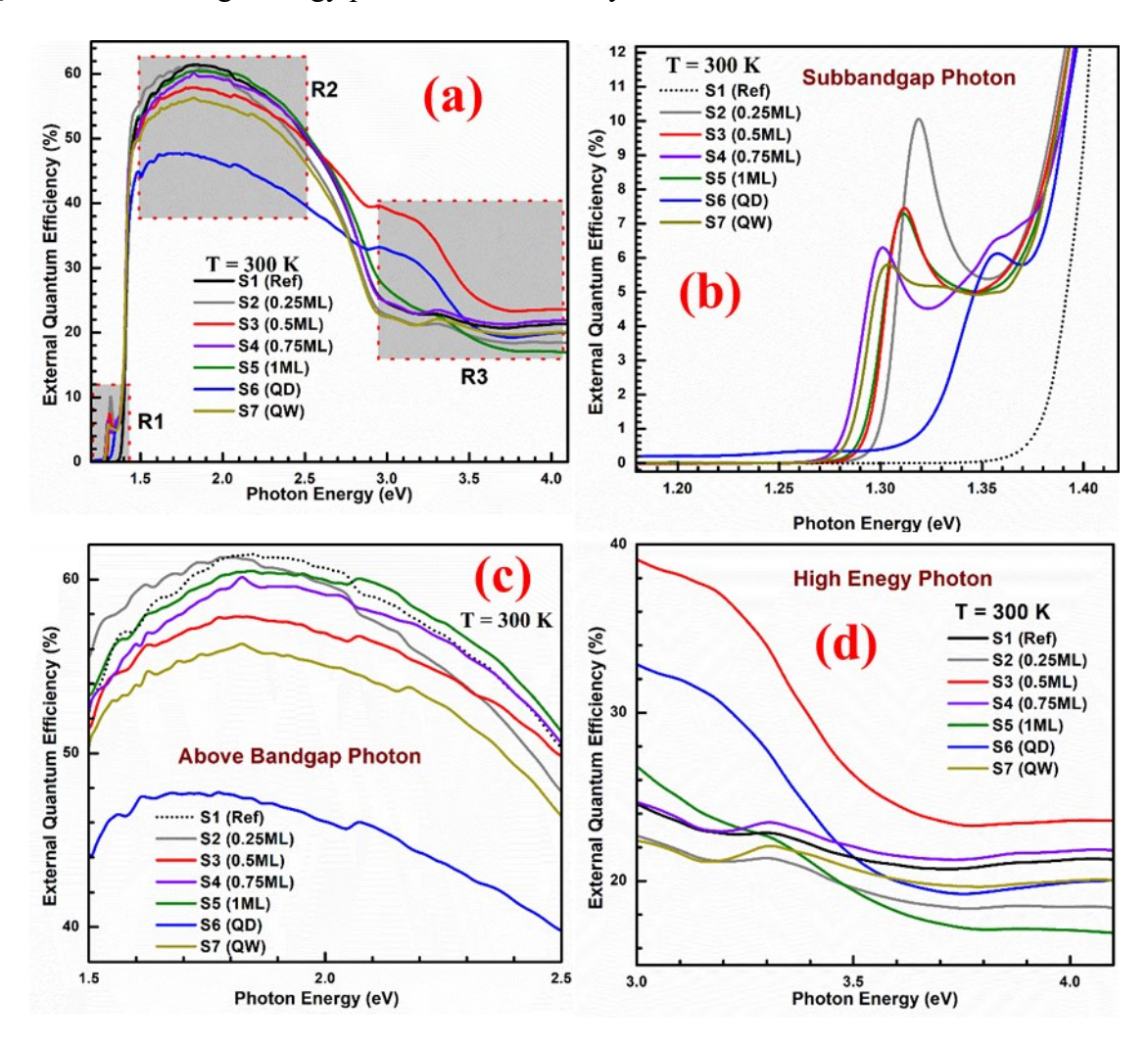


Fig. 3. EQE spectra of all samples (a) for broad wavelength range (shaded rectangles show three different regions); (b) for sub-bandgap photons; (c) for above bandgap photons; (d) for high energy photons.

## D. Illuminated I-V

The illuminated I-V characteristics for all samples are shown in Fig. 4. The open circuit voltage  $(V_{OC})$ , short-circuit current  $(I_{SC})$ , Fill factor (FF) and efficiency  $(\eta)$  of these devices are shown in Table 1. Compared to the reference solar cell, all other cells show a lower value of  $V_{OC}$ . However, the S2 (0.25 ML) sample shows only a negligible decrease in the  $V_{OC}$  compared to the reference SC. The observed  $V_{OC}$  degradation in all the SCs is due to the introduction of the smaller band gap (InAs) intermediate level, into the intrinsic region of the reference SC and the different

recombination mechanisms in the interband structures [23]–[25]. The discrete density of states in the SML QDs favor  $\Delta QFL$  which is a required condition to maintain  $V_{OC}$ . Additionally, the smaller size of the QDs compared to SK-QDs results in reduced carrier trapping. The SK-QD sample shows the lowest  $V_{OC}$  (even though the sample has the best material quality as indicated by XRD RC (Fig. 1(b)) due to carrier trapping by the large size of the QDs. In order to fully understand the  $V_{OC}$  degradation mechanism, a more comprehensive understanding of the recombination processes in these nanostructures is required.

Most of samples (except S4 and S6) show an enhanced short circuit current ( $I_{SC}$ ) due to the enhanced excess carriers by the sub-bandgap photon absorption. Carrier trapping in S6 and carrier recombination due to interface roughness between GaAs and InAs in S4 are the possible reasons for inferior  $I_{SC}$  in these samples. Interestingly, even with the poor material quality of S5 (1ML) sample, it shows significant enhancement in  $I_{SC}$  mainly because of smoother interface between GaAs and InAs [22].

Table 1. Solar cell device parameters

Sample ID	V <sub>OC</sub> (Volt)	I <sub>SC</sub> (mA)	FF	η (%)
S1 (Reference)	0.78	4.48	61.4	8.6
S2 (0.25ML)	0.78	4.88	69.1	10.6
S3 (0.5ML)	0.75	4.69	65.1	9.2
S4 (0.75ML)	0.69	4.46	57.8	7.1
S5 (1ML)	0.71	4.65	68.8	9.0
S6 (SK-QD)	0.59	4.23	59.6	6.0
S7 (QW)	0.69	4.66	68.9	8.9

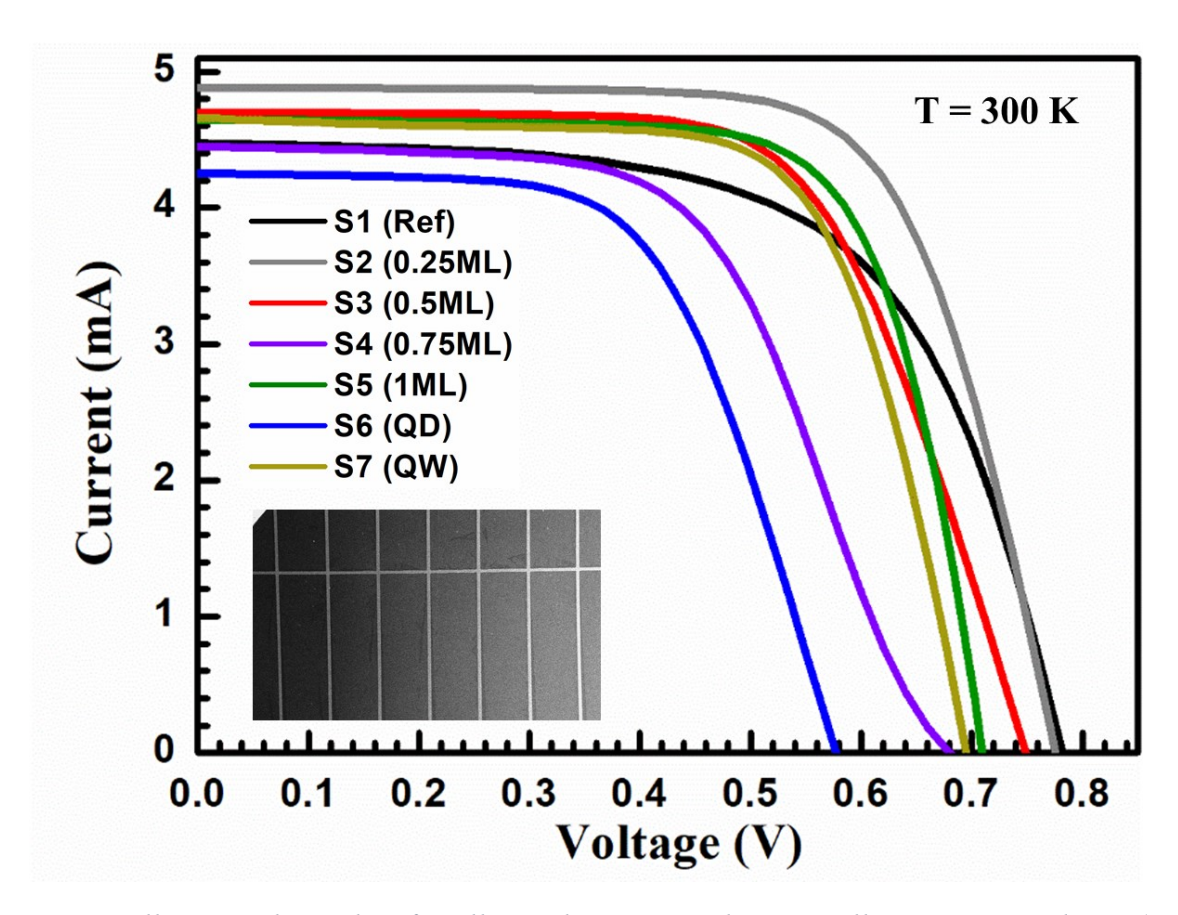


Fig. 4. Illuminated I-V plots for all samples at RT under 1 sun illumination condition (AM 1.5G, 100 mW/cm<sup>2</sup>); Inset shows the SEM image of top contacts of fabricated solar cell device.

#### 4. Conclusion:

We have investigated the structural, optical and electrical properties of different quantum structures (SK-QD, QW, SML-QD, quasi-ML InAs stack) in the active region of a pin junction SC. For the same InAs content, SK-QD shows the least defect formation whereas 1ML InAs stack shows the poorest material quality. PL results indicate strong confinement for 0.25 ML and 0.5 ML samples. Complementing its better optical properties, the 0.25 ML based SC shows the best EQE behavior indicating higher absorption of sub-bandgap photons, and subsequent efficient carrier extraction. Finally, the SML-QD based SC samples show significant enhancement in efficiency over reference SC mainly because of their high QD density and smaller QD size.

## **Acknowledgement:**

Authors acknowledge the financial support by the Institute for Nanoscience and Engineering, University of Arkansas, and the NSF grant number 1809054.

## References:

- [1] A. Luque and A. Martí, "Increasing the Efficiency of Ideal Solar Cells by Photon Induced Transitions at Intermediate Levels," *Phys. Rev. Lett.*, vol. 78, no. 26, pp. 5014–5017, Nov. 1997.
- [2] G. Wei, K. T. Shiu, N. C. Giebink, and S. R. Forrest, "Response to: Comment on 'Thermodynamic limits of quantum photovoltaic cell efficiency' [Appl. Phys. Lett. 92, 066101 (2008)]," *Applied Physics Letters*, vol. 92, no. 6. American Institute of PhysicsAIP, p. 066102, 11-Feb-2008.
- [3] G. Wei, K. T. Shiu, N. C. Giebink, and S. R. Forrest, "Thermodynamic limits of quantum photovoltaic cell efficiency," *Appl. Phys. Lett.*, vol. 91, no. 22, p. 223507, Nov. 2007.
- [4] S. Kettemann and J. F. Guillemoles, "Thermoelectric field effects in low-dimensional structure solar cells," *Phys. E Low-Dimensional Syst. Nanostructures*, vol. 14, no. 1–2, pp. 101–106, Apr. 2002.
- [5] S. P. Bremner, R. Corkish, and C. B. Honsberg, "Detailed balance efficiency limits with quasi-Fermi level variations," *IEEE Trans. Electron Devices*, vol. 46, no. 10, pp. 1932–1939, 1999.
- [6] N. G. Anderson, "On quantum well solar cell efficiencies," in *Physica E: Low-Dimensional Systems and Nanostructures*, 2002, vol. 14, no. 1–2, pp. 126–131.
- [7] A. Luque and A. Martí, "Increasing the Efficiency of Ideal Solar Cells by Photon Induced Transitions at Intermediate Levels," *Phys. Rev. Lett.*, vol. 78, no. 26, pp. 5014–5017, Nov. 1997.
- [8] K. W. J. Barnham and G. Duggan, "A new approach to high-efficiency multi-band-gap solar cells," *J. Appl. Phys.*, vol. 67, no. 7, pp. 3490–3493, Apr. 1990.
- [9] D. Guimard *et al.*, "Fabrication of InAs/GaAs quantum dot solar cells with enhanced photocurrent and without degradation of open circuit voltage," *Appl. Phys. Lett.*, vol. 96, no. 20, p. 203507, May 2010.
- [10] N. S. Beattie et al., "Quantum Engineering of InAs/GaAs Quantum Dot Based

- Intermediate Band Solar Cells," ACS Photonics, vol. 4, no. 11, pp. 2745–2750, Nov. 2017.
- [11] I. N. Stranski and L. Krastanow, "Zur Theorie der orientierten Ausscheidung von Ionenkristallen aufeinander," *Monatshefte für Chemie*, vol. 71, no. 1, pp. 351–364, Dec. 1937.
- [12] D. Zhou *et al.*, "Positioning effects on quantum dot solar cells grown by molecular beam epitaxy," *Appl. Phys. Lett.*, vol. 96, no. 8, p. 083108, Feb. 2010.
- [13] P. Lam *et al.*, "Submonolayer InGaAs/GaAs quantum dot solar cells," *Sol. Energy Mater. Sol. Cells*, vol. 126, pp. 83–87, Jul. 2014.
- [14] C. G. Bailey *et al.*, "Open-circuit voltage improvement of InAs/GaAs quantum-dot solar cells using reduced InAs coverage," *IEEE J. Photovoltaics*, vol. 2, no. 3, pp. 269–275, 2012.
- [15] V. P. Kunets *et al.*, "InGaAs quantum wire intermediate band solar cell," *Appl. Phys. Lett.*, vol. 101, no. 4, p. 041106, Jul. 2012.
- [16] S. M. Willis *et al.*, "Defect mediated extraction in InAs/GaAs quantum dot solar cells," *Sol. Energy Mater. Sol. Cells*, vol. 102, pp. 142–147, Jul. 2012.
- [17] J. S. Wang, J. F. Chen, J. L. Huang, P. Y. Wang, and X. J. Guo, "Carrier distribution and relaxation-induced defects of InAs/GaAs quantum dots," *Appl. Phys. Lett.*, vol. 77, no. 19, pp. 3027–3029, Nov. 2000.
- [18] I. S. Han, J. S. Kim, J. O. Kim, S. K. Noh, and S. J. Lee, "Fabrication and characterization of InAs/InGaAs sub-monolayer quantum dot solar cell with dot-in-a-well structure," *Curr. Appl. Phys.*, vol. 16, no. 5, pp. 587–592, May 2016.
- [19] G. S. Solomon, J. A. Trezza, and J. S. Harris, "Effects of monolayer coverage, flux ratio, and growth rate on the island density of InAs islands on GaAs," *Appl. Phys. Lett.*, vol. 66, no. 23, p. 3161, Jun. 1995.
- [20] G. S. Solomon, J. A. Trezza, and J. S. Harris, "Substrate temperature and monolayer coverage effects on epitaxial ordering of InAs and InGaAs islands on GaAs," *Appl. Phys. Lett.*, vol. 66, no. 8, p. 991, Feb. 1995.

- [21] Z. Xu *et al.*, "Structure and optical anisotropy of vertically correlated submonolayer InAs/GaAs quantum dots," *Appl. Phys. Lett.*, vol. 82, no. 22, pp. 3859–3861, Jun. 2003.
- [22] R. Kumar *et al.*, "Excitation intensity and thickness dependent emission mechanism from an ultrathin InAs layer in GaAs matrix," *J. Appl. Phys.*, vol. 124, no. 23, p. 235303, Dec. 2018.
- [23] A. Luque, A. Martí, and C. Stanley, "Understanding intermediate-band solar cells," *Nat. Photonics*, vol. 6, no. 3, pp. 146–152, Mar. 2012.
- [24] S. M. Sze, *Physics of Semiconductor Devices, 3rd Edition* | Wiley. 1981.
- [25] D. K. Schroder, Semiconductor Material and Device Characterization, 3rd Edition | Wiley. NJ: John Wiley & Sons, NJ, 2006.